A&A 383, 1076–1087 (2002)
DOI: 10.1051/0004-6361:20011797

Astronomy & Astrophysics

Three types of cooling superfluid neutron stars: Theory and observations

A. D. Kaminker[1], D. G. Yakovlev[1], and O. Y. Gnedin[2]

[1] Ioffe Physical Technical Institute, Politekhnicheskaya 26, 194021 St. Petersburg, Russia
[2] Space Telescope Science Institute, 3700 San Martin Drive, Baltimore, MD 21218, USA
e-mail: yak@astro.ioffe.rssi.ru; ognedin@stsci.edu

Received 21 November 2001 / Accepted 17 December 2001

Abstract. Cooling of neutron stars (NSs) with the cores composed of neutrons, protons, and electrons is simulated assuming $^1S_0$ pairing of neutrons in the NS crust, and also $^1S_0$ pairing of protons and weak $^3P_2$ pairing of neutrons in the NS core, and using realistic density profiles of the superfluid critical temperatures $T_c(\rho)$. The theoretical cooling models of isolated middle-aged NSs can be divided into three main types. (I) *Low-mass*, *slowly cooling* NSs where the direct Urca process of neutrino emission is either forbidden or almost fully suppressed by the proton superfluidity. (II) *Medium-mass* NSs which show *moderate* cooling via the direct Urca process suppressed by the proton superfluidity. (III) *Massive* NSs which show *fast* cooling via the direct Urca process weakly suppressed by superfluidity. Confronting the theory with observations we treat RX J0822–43, PSR 1055–52 and RX J1856–3754 as slowly cooling NSs. To explain these sufficiently warm sources we need a density profile $T_c(\rho)$ in the crust with a rather high and flat maximum and sharp wings. We treat 1E 1207–52, RX J0002+62, PSR 0656+14, Vela, and Geminga as moderately cooling NSs. We can determine their masses for a given model of proton superfluidity, $T_{cp}(\rho)$, and the equation of state in the NS core. No rapidly cooling NS has been observed so far.

Key words. stars: neutron – dense matter

1. Introduction

Cooling of neutron stars (NSs) depends on the properties of matter of subnuclear and supranuclear density in the NS crusts and cores. These properties are still poorly known and cannot be predicted precisely by contemporary microscopic theories. For instance, microscopic calculations of the equation of state (EOS) of matter in the NS cores (e.g., Lattimer & Prakash 2001) or the superfluid properties of NS cores and crusts (e.g., Lombardo & Schulze 2001) show a large scatter of results depending on a model of strong interaction and a many-body theory employed. It is important that these properties can be studied by confronting the results of simulations of NS cooling with the observations of thermal emission from isolated middle-aged NSs.

This paper is devoted to such studies. For simplicity, we use the NS models with the cores composed of neutrons (n) with an admixture of protons (p) and electrons. We will mainly focus on the superfluid properties of NS matter which are characterized by the density-dependent critical temperatures $T_c(\rho)$ of nucleons. It is customary to consider superfluidities of three types: singlet-state ($^1S_0$) superfluidity ($T_c = T_{cns}$) of neutrons in the inner NS crust and the outermost core; $^1S_0$ proton superfluidity in the core ($T_c = T_{cp}$); and triplet-state ($^3P_2$) neutron superfluidity in the core ($T_c = T_{cnt}$). Superfluidity of nucleons suppresses neutrino processes involving nucleons and affects nucleon heat capacities (e.g., Yakovlev et al. 1999). In addition, it initiates a specific mechanism of neutrino emission associated with Cooper pairing of nucleons (Flowers et al. 1976). Our aim is to analyze which critical temperatures $T_c(\rho)$ are consistent with observations and do not contradict the current microscopic calculations.

We have considered this problem in two prior publications. Kaminker et al. (2001, hereafter Paper I) analyzed the effects of proton superfluidity (basing on one particular model of $T_{cp}(\rho)$) and $^3P_2$ neutron superfluidity in the NS core. Yakovlev et al. (2001, hereafter Paper II) included, additionally, the effects of $^1S_0$ neutron superfluidity in the crust. Calculations in Papers I and II were performed for one particular EOS in the NS core. In the present paper we extend the results of Papers I and II by considering three models of proton superfluidity and another EOS in the NS core. We combine the results of Papers I and II and give an overall analysis of the problem. We show that one can distinguish *three* distinctly different types of isolated middle-aged NSs, which show *slow*,

Send offprint requests to: A. D. Kaminker,
e-mail: kam@astro.ioffe.rssi.ru

moderate, and *fast* cooling. Using this concept we discuss a possible interpretation of observations of thermal emission from eight middle-aged isolated NSs.

2. Cooling models

We simulate NS cooling with our fully relativistic non-isothermal cooling code (Gnedin et al. 2001). The code solves the radial heat diffusion equation in the NS interior (excluding the outer heat-blanketing layer placed at $\rho < 10^{10}$ g cm^{-3}). The heat is carried away by the neutrino emission from the entire stellar body and by the thermal photon emission from the surface. No additional reheating mechanisms are included.

The code calculates theoretical cooling curves, i.e., the effective surface temperature as detected by a distant observer, $T_{\rm s}^{\infty}$, versus NS age t. The thermal history of an isolated NS consists of three stages. The first is the stage of thermal relaxation of the stellar interior (e.g., Lattimer et al. 1994; Gnedin et al. 2001). It lasts for about 10–100 yr. It is followed by the stage at which the NS interior is isothermal and the neutrino luminosity exceeds the surface photon luminosity ($t \lesssim (3-10)\times 10^5$ yr). The final stage is the photon cooling stage at which the photon luminosity dominates the neutrino one.

In the NS crust we use the EOS of Negele & Vautherin (1973) (atomic nuclei everywhere in the crust are assumed to be spherical). The core-crust interface is placed at the density 1.5×10^{14} g cm^{-3}. A standard procedure is used to match the core and crust EOSs near the core-crust interface. In the core, we use two phenomenological EOSs proposed by Prakash et al. (1988). We refer to them as EOS A and EOS B.

EOS A is model I of Prakash et al. (1988) with the compression modulus of saturated nuclear matter $K = 240$ MeV. It has been used in Papers I and II. EOS B corresponds to $K = 180$ MeV and to the simplified form of the symmetry energy proposed by Page & Applegate (1992). EOS B has been used in a number of papers (e.g., Page & Applegate 1992; Yakovlev et al. 1999, and references therein).

The masses, central densities, and radii of two stellar configurations for each EOS are given in Table 1. The first configuration is the most massive stable NS. The values of $M_{\rm max}$ indicate that EOS A is stiff while EOS B is moderate. The second configuration has a central density at which the direct Urca process switches on; for both EOSs it is allowed at $M > M_{\rm D}$ ($\rho_{\rm c} > \rho_{\rm D}$). EOS B implies a smaller symmetry energy at supranuclear densities and opens the direct Urca process at a higher density.

Our cooling code includes all the important neutrino emission processes in the NS core (direct and modified Urca, neutrino bremsstrahlung in nucleon-nucleon collisions, neutrino emission due to Cooper pairing of nucleons) and in the crust (plasmon decay, neutrino bremsstrahlung due to scattering of electrons off atomic nuclei, electron-positron annihilation into neutrino pairs, neutrino emission due to Cooper pairing of free neutrons in the inner crust). The effects of nucleon superfluidity are incorporated in the neutrino reaction rates and nucleon heat capacities as described in Yakovlev et al. (1999, 2001). The effective masses of protons and neutrons in the core and free neutrons in the crust are taken to be 0.7 of the bare nucleon masses. The values of the thermal conductivity in the NS crust and core are the same as used by Gnedin et al. (2001).

Table 1. NS models employing EOSs A and B.

Model	Main parameters	EOS A	EOS B
Maximum mass model	$M_{\rm max}/M_\odot$	1.977	1.73
	$\rho_{\rm cmax}/10^{14}$ g cm^{-3}	25.75	32.5
	R km	10.754	9.71
Direct Urca threshold model	$M_{\rm D}/M_\odot$	1.358	1.44
	$\rho_{\rm D}/10^{14}$ g cm^{-3}	7.851	12.98
	R km	12.98	11.54

The relationship between the effective surface temperature and the temperature at the bottom of the outer heat-blanketing envelope is taken according to Potekhin et al. (1997) and Potekhin & Yakovlev (2001). This allows us to consider either the models of NSs with the surface layers made of iron, without magnetic field and with the dipole surface magnetic fields $B \lesssim 10^{15}$ G, or the non-magnetic NS models with the surface layers containing light elements. It is assumed that the surface magnetic field induces an anisotropic heat transport in the heat-blanketing envelope but does not violate the isotropic (radial) heat diffusion in the deeper NS layers. It is also assumed that a NS may have a hydrogen atmosphere even if the heat-blanketing envelope is mostly made of iron. The majority of cooling curves will be calculated for the model of non-magnetized heat-blanketing envelope made of iron. Two exceptions are considered in Sect. 4.3.

Although the microscopic calculations of superfluid critical temperatures $T_{\rm c}(\rho)$ give a large scatter of results (Sect. 1), some common features are evident. For instance, $T_{\rm c}(\rho)$ increases with ρ at sufficiently low densities (due to an increasing strength of the attractive part of nucleon-nucleon interaction), reaches maximum and then decreases (due to a short-range nucleon-nucleon repulsion) vanishing at a rather high density. For $T_{\rm cns}(\rho)$, the maximum takes place at subnuclear densities, while the switch off occurs at $\rho \sim \rho_0$, where $\rho_0 \approx 2.8 \times 10^{14}$ g cm^{-3} is the saturated nuclear matter density. For $T_{\rm cp}(\rho)$ and $T_{\rm cnt}(\rho)$, the maxima take place at a few ρ_0 and the fall occurs at the densities several times higher. The maximum values of $T_{\rm c}$ range from about 10^8 K (or even lower) to $(2-3)\times 10^{10}$ K, depending on the microscopic theoretical model employed. The maximum values of $T_{\rm cnt}$ are typically lower than those of $T_{\rm cp}$ and $T_{\rm cns}$, due to the weaker nucleon-nucleon attraction in the ^{3}P$_2$ state.

Instead of studying $T_{\rm c}$ as a function of ρ, it is often convenient to consider it versus the nucleon Fermi wavenumber $k = k_{\rm FN} = (3\pi^2 n_{\rm N})^{1/3}$, where $n_{\rm N}$ is the number density of nucleon species N = n or p. Moreover, instead of

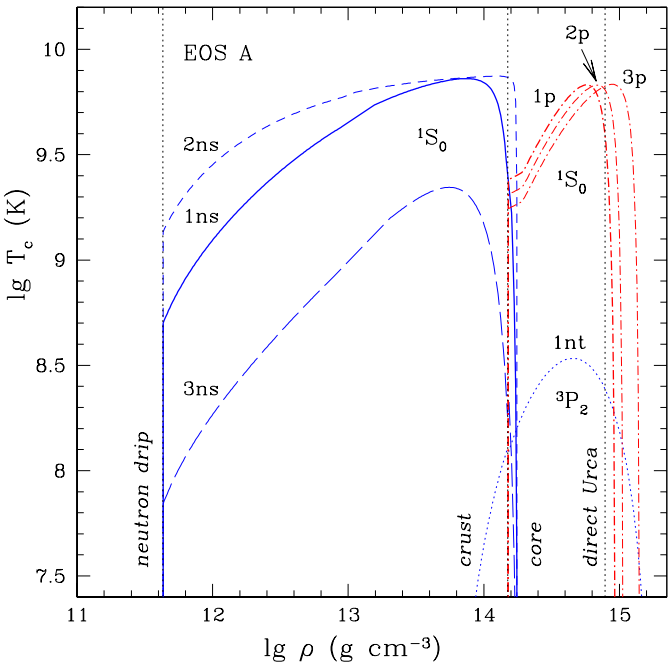

Fig. 1. Density dependence of the critical temperatures for three models 1p, 2p, and 3p of the proton superfluidity (dots-and-dashes) in the core (with EOS A); three models 1ns, 2ns, and 3ns of $^1S_0$ neutron superfluidity (solid, short-dashed, and long-dashed lines); and one model 1nt of $^3P_2$ neutron superfluidity (dots) used in cooling simulations. The parameters of the models are given in Table 2. Vertical dotted lines indicate neutron drip point, core-crust interface, and the direct Urca threshold.

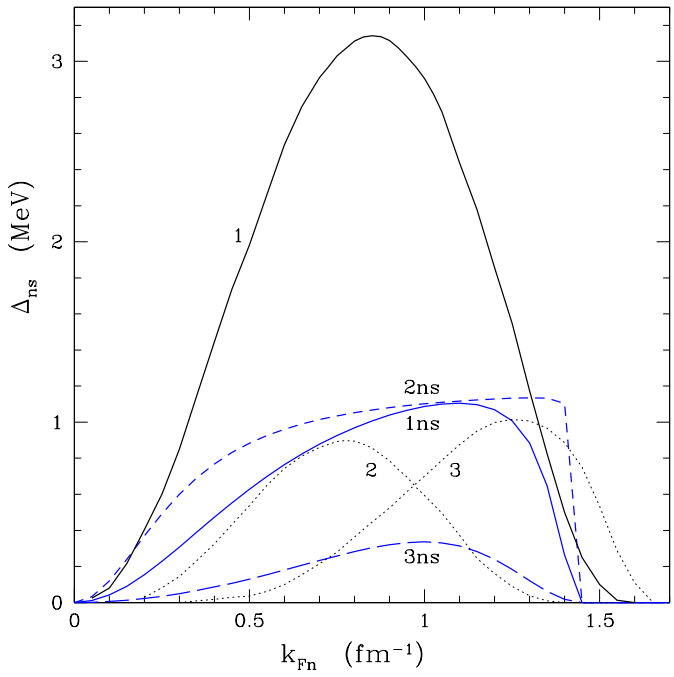

Fig. 2. Superfluid gaps for $^1S_0$ neutron pairing versus neutron Fermi wavenumber k_{Fn} for models 1ns, 2ns, and 3ns (solid line 1ns, short-dashed line 2ns, and long-dashed line 3ns; Fig. 1, Table 2). Solid line 1 is the gap derived from the BCS theory with in-vacuum nn interaction (after Lombardo & Schulze 2001); dotted lines 2 and 3 are two different theoretical curves obtained by Wambach et al. (1993) and Schulze et al. (1996) including medium polarization effects.

$T_c(k)$ one often considers $\Delta(k)$, the zero-temperature superfluid gap. For the $^1S_0$ pairing, assuming BCS theory, one has $\Delta(k) = T_c(k)/0.5669$. In the case of $^3P_2$ neutron pairing the gap depends on the orientation of nucleon momenta with respect to the quantization axis. Following the majority of papers we adopt the $^3P_2$ pairing with zero projection of the total angular momentum on the quantization axis. In that case $\Delta_{nt}(k) = T_{cnt}(k)/0.8416$, where $\Delta_{nt}(k)$ is the minimum value of the gap on the neutron Fermi surface (corresponding to the equator of the Fermi sphere; e.g., Yakovlev et al. 1999).

Taking into account a large scatter of $T_c(k)$ provided by microscopic theories we do not rely on any particular microscopic model. Following Papers I and II, we parameterize T_c as

$$T_c = T_0 \frac{(k-k_0)^2}{(k-k_0)^2+k_1^2} \frac{(k-k_2)^2}{(k-k_2)^2+k_3^2}, \quad (1)$$

for $k_0 < k < k_2$; and $T_c = 0$, for $k \le k_0$ or $k \ge k_2$. The factor T_0 regulates the amplitude of T_c, k_0 and k_2 determine positions of the low- and high-density cutoffs, while k_1 and k_3 specify the shape of $T_c(\rho)$. All wavenumbers, k, $k_0, \ldots k_3$ will be expressed in fm^{-1}. We have verified that by tuning T_0, k_0, $\ldots k_3$, our parameterization describes accurately numerous results of microscopic calculations.

In our cooling simulations we consider three models of $^1S_0$ proton superfluidity, three models of $^1S_0$ neutron superfluidity, and one model of $^3P_2$ neutron superfluidity. The parameters of the models are given in Table 2, and the appropriate $T_c(\rho)$ are plotted in Fig. 1. We have $k_0 = 0$ for $^1S_0$ pairing. At any given ρ we choose the neutron superfluidity ($^1S_0$ or $^3P_2$) with higher T_c.

Table 2. Parameters of superfluid models in Eq. (1).

Pairing	Model	$T_0/10^9$ K	k_0 fm^{-1}	k_1 fm^{-1}	k_2 fm^{-1}	k_3 fm^{-1}
$^1S_0$	1p	20.29	0	1.117	1.241	0.1473
$^1S_0$	2p	17	0	1.117	1.329	0.1179
$^1S_0$	3p	14.5	0	1.117	1.518	0.1179
$^1S_0$	1ns	10.2	0	0.6	1.45	0.1
$^1S_0$	2ns	7.9	0	0.3	1.45	0.01
$^1S_0$	3ns	1800	0	21	1.45	0.4125
$^3P_2$	1nt	6.461	1	1.961	2.755	1.3

Models 1ns, 2ns, and 3ns of $^1S_0$ neutron superfluidity are the same as used in Paper II. Models 1ns and 2ns correspond to about the same, rather strong superfluidity (with maximum $T_{cns} \approx 7 \times 10^9$ K). Model 2ns has flatter maximum and sharper decreasing slopes in the wings (near the crust-core interface and the neutron drip point). Model 3ns represents a much weaker superfluidity, with maximum $T_{cns} \approx 2.4 \times 10^9$ K and a narrower density profile. (One can visualize the radial distributions of T_c in a NS by comparing the horizontal scales in Figs. 1 and 4.)

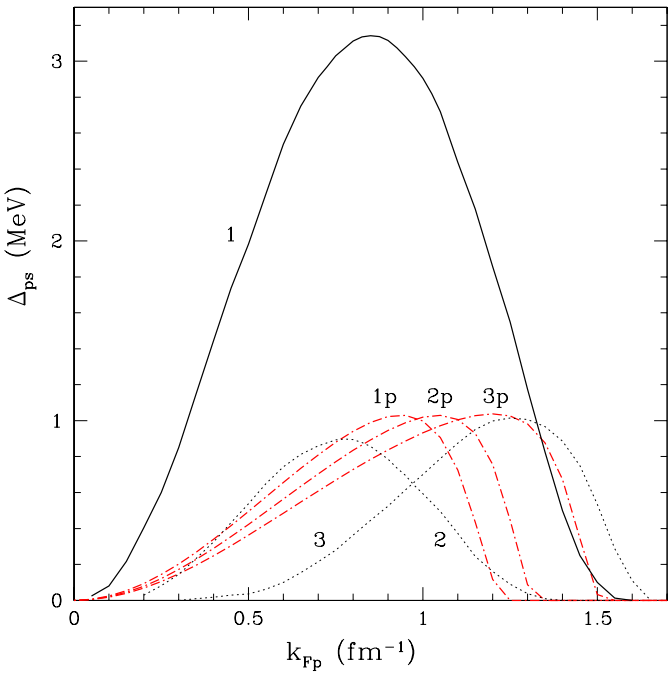

Fig. 3. Superfluid gaps for models 1p, 2p, and 3p (Fig. 1, Table 2) of proton pairing (dot-and-dashed lines) versus proton Fermi wavenumber. Solid line 1 and dotted lines 2 and 3 are the same as in Fig. 2.

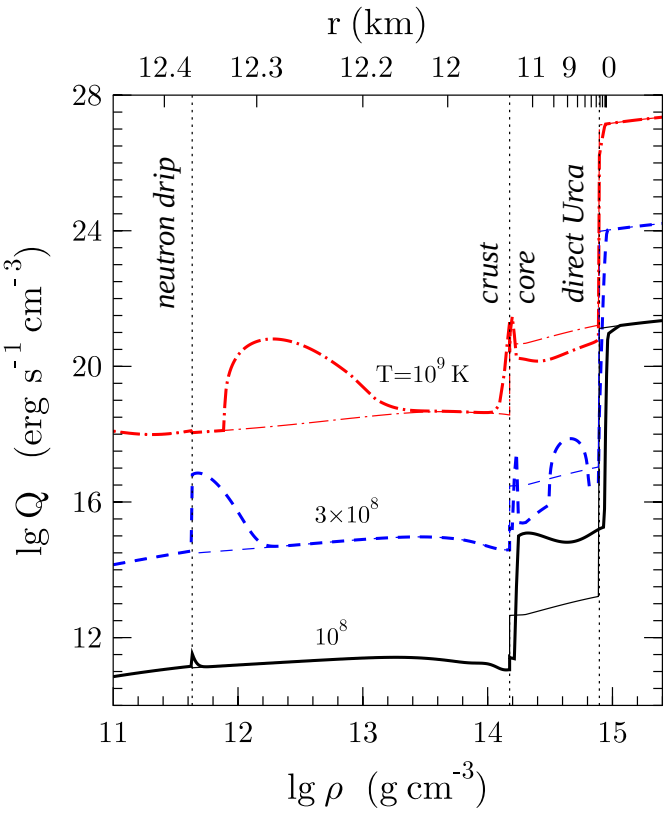

Fig. 4. Total neutrino emissivity versus density (lower horizontal scale) for $T = 10^8$ (solid lines), 3×10^8 (dashes), and 10^9 K (dot-and-dashes) assuming EOS A at supranuclear densities. Thin lines are for non-superfluid matter; thick lines are for matter with 1ns, 1nt, and 1p superfluids of neutrons and protons. Vertical dotted lines are the same as in Fig. 1. Upper horizontal scale shows the radial coordinate r in a 1.5 $M_\odot$ NS.

The superfluid gaps for these models are shown in Fig. 2 versus the neutron Fermi wavenumber. For comparison, we present also three curves provided by microscopic theories. Solid curve 1 is obtained using BCS theory with the in-vacuum nn-interaction (after Lombardo & Schulze 2001). This approach yields a very strong superfluidity with the maximum gap $\Delta_{ns} \approx 3$ MeV. Dotted curves 2 and 3 are calculated using two different models of nn-interaction affected by the medium polarization (Wambach et al. 1993; Schulze et al. 1996). The polarization effects strongly reduce the gaps. Microscopic models of $\Delta_{ns}(k)$ are abundant in the literature and the results differ considerably (see, e.g., Fig. 7 in Lombardo & Schulze 2001 or Fig. 3 in Yakovlev et al. 1999). Our phenomenological curves 1ns, 2ns, and 3ns all fall in the range covered by theoretical curves. The shapes of the $\Delta_{ns1}(k)$ and $\Delta_{ns3}(k)$ curves are typical whereas the decrease of $\Delta_{ns2}(k)$ with k at $k \gtrsim 1.4$ fm^{-1} is not (too sharp).

The proton superfluidity curves 1p, 2p, and 3p in Fig. 1 are similar. The maximum values of T_{cp} are about 7×10^9 K for all three models. Note that model 1p was used in Papers I and II. The models differ by the positions of the maximum and decreasing slopes of $T_{cp}(\rho)$. The decreasing slope of model 1p is slightly above the threshold density of the direct Urca process (for EOS A), while the slopes for models 2p and 3p are shifted to a higher ρ. The corresponding gaps are shown in Fig. 3. For comparison, in Fig. 3 we present the same curves 1, 2, and 3 as in Fig. 2 (the proton gap $\Delta_{ps}(k_{Fp})$ is expected to be similar to the neutron gap $\Delta_{ns}(k_{Fn})$). Our models 1p, 2p, and 3p are typical for those microscopic theories which adopt a moderately strong medium polarization of pp-interaction.

Finally, the dotted curve in Fig. 1 shows $T_{cnt}(\rho)$ for our model 1nt of $^3P_2$ neutron pairing (used in Paper I). Microscopic theories give a very large scatter of $T_{cnt}(\rho)$, and our curve falls within their limits.

Figure 4 shows the density profile of the neutrino emissivity at $T = 10^8$, 3×10^8, and 10^9 K. Thin lines correspond to non-superfluid matter and have three distinct parts. In the crust, the emissivity is mainly produced by neutrino bremsstrahlung due to the scattering of electrons off nuclei. In the outer core, the emissivity is mainly produced by the modified Urca process and is about two orders of magnitude higher. In the inner core, it is due to the direct Urca process and is higher by another 6–7 magnitudes. Thick lines are for superfluid matter (1ns, 1nt, and 1p superfluids of neutrons and protons). At $T = 10^9$ K there are two large emissivity peaks, near the neutron drip-point and the crust-core interface. They are associated with the neutrino emission due to $^1S_0$ Cooper pairing of neutrons. They are explained by the fact that the Cooper-pairing neutrino emissivity is most intense at $0.8\,T_c \lesssim T \leq T_c$,

Table 3. Surface temperatures of eight isolated middle-aged neutron stars inferred from observations.

Source	lg t [yr]	lg $T_{\rm s}^{\infty}$ [K]	Model[a)]	Confid. level	References
RX J0822–43	3.57	$6.23^{+0.02}_{-0.02}$	H	95.5%	Zavlin et al. (1999)
1E 1207–52	3.85	$6.10^{+0.05}_{-0.06}$	H	90%	Zavlin et al. (1998)
RX J0002+62	3.95[b)]	$6.03^{+0.03}_{-0.03}$	H	95.5%	Zavlin & Pavlov (1999)
PSR 0833–45 (Vela)	4.4[c)]	$5.83^{+0.02}_{-0.02}$	H	68%	Pavlov et al. (2001)
PSR 0656+14	5.00	$5.96^{+0.02}_{-0.03}$	bb	90%	Possenti et al. (1996)
PSR 0633+1748 (Geminga)	5.53	$5.75^{+0.05}_{-0.08}$	bb	90%	Halpern & Wang (1997)
PSR 1055–52	5.73	$5.88^{+0.03}_{-0.04}$	bb	[d)]	Ögelman (1995)
RX J1856–3754	5.95	$5.72^{+0.05}_{-0.06}$	[e)]	[d)]	Pons et al. (2001)

[a)] Observations are interpreted either with a hydrogen atmosphere model (H), or with a black body spectrum (bb).

[b)] The mean age taken according to Craig et al. (1997).

[c)] According to Lyne et al. (1996).

[d)] Confidence level is uncertain.

[e)] Analytic fit with Si-ash atmosphere model of Pons et al. (2001).

and is exponentially small at $T \ll T_{\rm c}$ (e.g., Yakovlev et al. 1999). One can also see a reduction of neutrino emission in the outer core by the proton superfluidity. The same superfluidity reduces also the direct Urca process near its threshold, $\rho \gtrsim \rho_{\rm D}$, but becomes weaker (Fig. 1) and has no effect at higher densities. At $T = 3 \times 10^8$ K the peaks associated with ^{1}S$_0$ neutron pairing are weaker, but there is a new high peak in the outer core due to ^{3}P$_2$ neutron pairing. At $T = 10^8$ K the neutrino emission due to ^{1}S$_0$ neutron pairing almost disappears but the emission due to ^{3}P$_2$ pairing persists. At still lower temperature, the ^{3}P$_2$-pairing emissivity in the outer core will have two peaks and gradually disappear. Upper horizontal scale gives the radial coordinate in a 1.5 $M_\odot$ NS. The bulk of neutrino emission comes evidently from the core (∼11 km in radius), and a lower fraction comes from the crust (∼1 km thick).

The results of cooling calculations are illustrated in Figs. 5–10 and described in Sect. 4.

3. Observational data

We will confront theoretical cooling curves with the results of observations of thermal emission from eight middle-aged isolated NSs. The observational data are the same as in Papers I and II. They are summarized in Table 3 and displayed in Figs. 5–7 and 10. The three youngest objects (RX J0822–43, 1E 1207–52, and RX J0002+62) are radio-quiet NSs in supernova remnants. The oldest object, RX J1856–3754, is also a radio-quiet NS. The other objects, Vela, PSR 0656+14, Geminga, and PSR 1055–52, are observed as radio pulsars. The NS ages are either pulsar spindown ages or the estimated supernova ages. The age of RX J1856–3754 was estimated by Walter (2001) from the kinematical data (by identifying a possible pre-supernova companion in the binary system). We use the value $t = 9 \times 10^5$ yr mentioned in the subsequent publication by Pons et al. (2001).

For the four youngest sources, the effective surface temperatures $T_{\rm s}^{\infty}$ are obtained from the observed X-ray spectra using hydrogen atmosphere models. Such models are more consistent with other information on these sources (distances, hydrogen column densities, inferred NS radii, etc.) than the blackbody model of NS emission. On the contrary, for the next three sources we present the values of $T_{\rm s}^{\infty}$ inferred using the blackbody spectrum because the blackbody model is more consistent for these sources. Finally, for RX J1856–3754 we adopt the values inferred using the analytic fit with Si-ash atmosphere model of Pons et al. (2001). We expect that the large errorbar of $T_{\rm s}^{\infty}$ provided by this model reflects poor understanding of thermal emission from this source (e.g., Pons et al. 2001; Burwitz et al. 2001; Gänsicke et al. 2001; Kaplan et al. 2001).

4. Theory versus observations

4.1. General remarks

We have a large scatter of observational limits on $T_{\rm s}^{\infty}$ for the eight sources. Three sources, the youngest RX J0822–43, and two oldest, PSR 1055–52 and

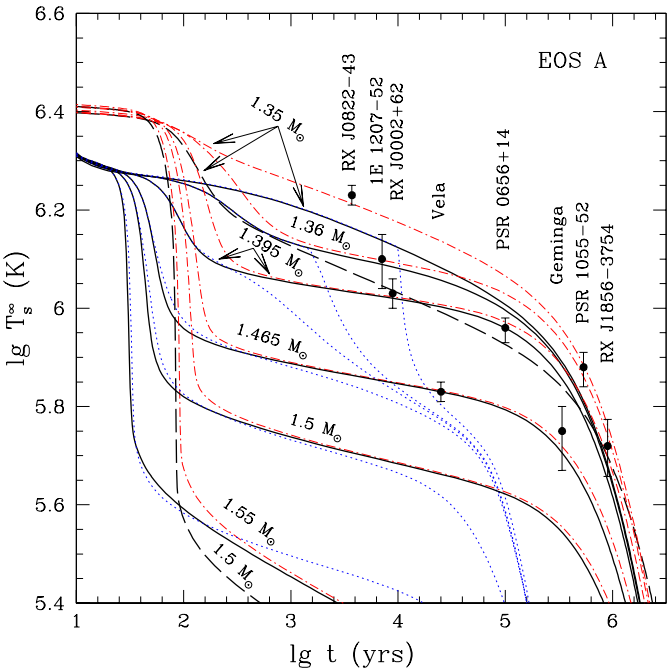

Fig. 5. Observational limits on surface temperatures of eight NSs (Table 3) compared with cooling curves for NS models (EOS A) with masses from 1.35 to 1.55 $M_\odot$. Dot-and-dashed curves are obtained including proton superfluidity 1p alone. Solid curves include, in addition, model 1ns of neutron superfluidity. Dotted lines also take into account the effect of neutron superfluidity 1nt. Long-dashed lines are for non-superfluid 1.35 and 1.5 $M_\odot$ NSs.

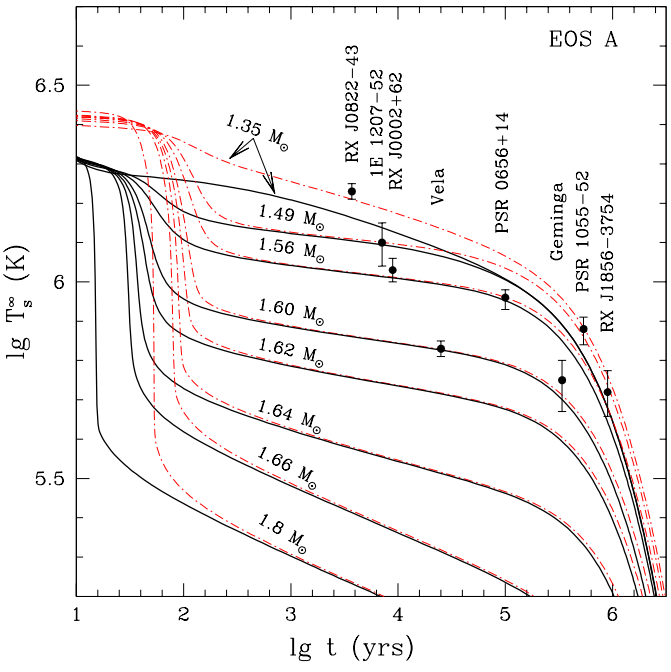

Fig. 6. Observational limits on surface temperatures of NSs compared with cooling curves for NS models (EOS A) with several masses M in the presence of proton superfluidity 2p. Dot-and-dashed curves are obtained assuming non-superfluid neutrons. Solid curves include, in addition, model 1ns of neutron superfluidity. $^3P_2$ neutron pairing is neglected.

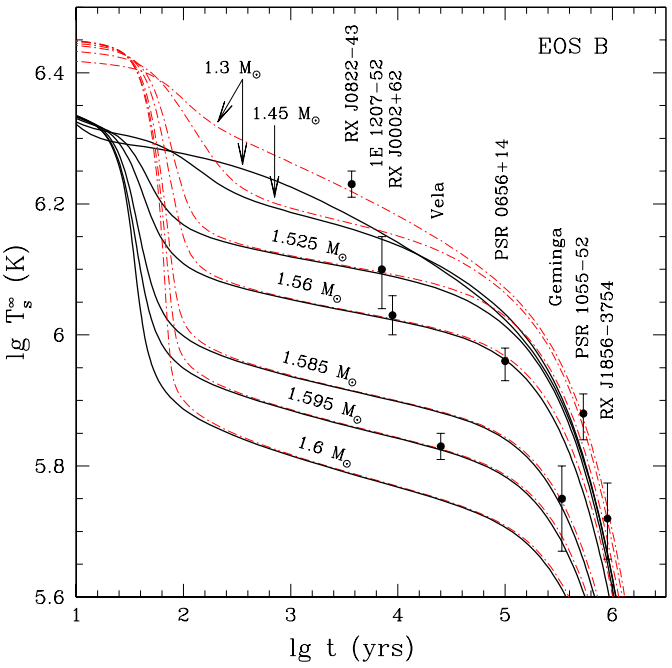

Fig. 7. Observational limits on surface temperatures of NSs compared with cooling curves for NS models (EOS B) with masses from 1.3 to 1.6 $M_\odot$. Dot-and-dashed curves are obtained using model 3p of proton superfluidity. Solid curves include, in addition, model 1ns of neutron superfluidity.

RX J1856–3754, seem to be hot for their ages, while the other ones, especially Vela and Geminga, look much colder. Our aim is to interpret all observational data with the cooling curves using the fixed (the same) EOS and models of the critical temperatures $T_c(\rho)$ (Sect. 2) for all objects. The results are presented in Figs. 5–10.

In the *absence of any superfluidity* we would have *two* well-known, distinctly different cooling regimes, *slow* and *fast* cooling. The slow cooling takes place in low-mass NSs, with $M < M_D$. In middle-aged NSs, it goes mainly via neutrino emission produced by modified Urca processes. For a given EOS in the NS core, the cooling curves of middle-aged NSs are almost the same for all M from about 1.1 $M_\odot$ to M_D (e.g., Page & Applegate 1992; Gnedin et al. 2001), and they are not very sensitive to EOS. The fast cooling occurs if $M > M_D + 0.003\,M_\odot$ via a very powerful direct Urca process (Lattimer et al. 1991). The cooling curves are again not too sensitive to the mass and EOS. The middle-aged rapidly cooling NSs are much colder than the slowly cooling ones. Two examples, for 1.35 and 1.5 $M_\odot$ non-superfluid NSs (EOS A), are displayed in Fig. 5 by long dashes. The transition from the slow to fast cooling takes place in a very narrow range of M. It is demonstrated in Fig. 8 which shows T_s^∞ versus NS mass at the age $t = 2.5 \times 10^4$ yr of the Vela pulsar. Horizontal dotted lines show observational limits on T_s^∞ for the Vela pulsar. One can see a very sharp fall of T_s^∞ in the mass range $M_D < M \lesssim M_D + 0.003\,M_\odot$ for non-superfluid NSs

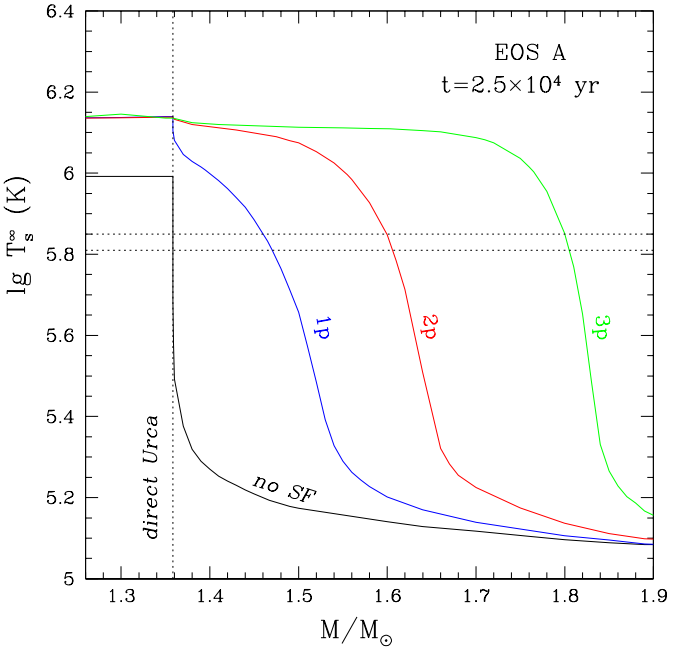

Fig. 8. Surface temperatures of NS models (EOS A) at $t = 2.5 \times 10^4$ yr, the age of the Vela pulsar, versus stellar mass M. The curves are calculated (from bottom to top) assuming either no superfluidity, or proton superfluidities 1p, 2p, 3p (and neglecting neutron superfluidity). The vertical dotted line shows the threshold mass $M_{\rm D}$ of opening the direct Urca process. Horizontal dotted lines are observational limits on the Vela's surface temperature (Table 3).

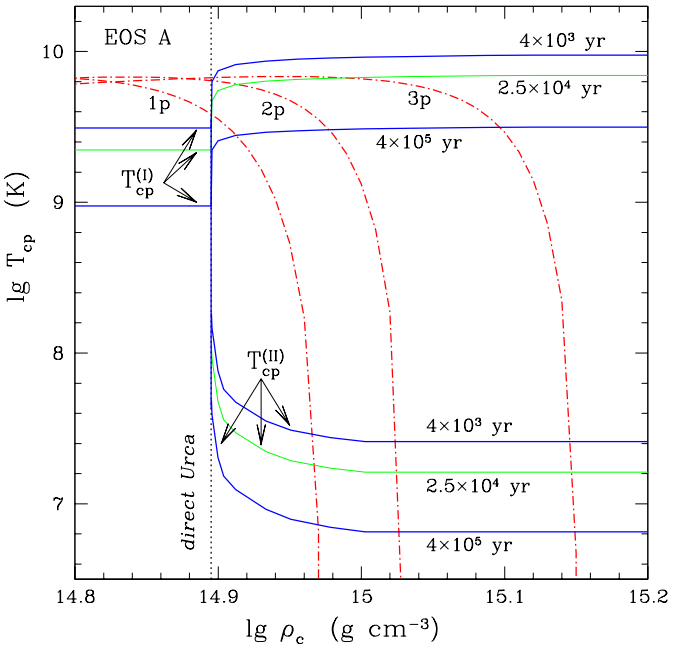

Fig. 9. Two characteristic critical temperatures of proton superfluidity, $T_{\rm cp}^{\rm (I)}$ and $T_{\rm cp}^{\rm (II)}$, versus NS central density $\rho_{\rm c}$ for EOS A and three NS ages, 4×10^3, 2.5×10^4, and 4×10^5 yr. Also shown are $T_{\rm cp}(\rho)$ (dot-and-dashed) curves for proton superfluids 1p, 2p, and 3p. Their intersections with $T_{\rm cp}^{\rm (I,II)}$ at $\rho_{\rm c} \geq \rho_{\rm D}$ separates the low-, medium-, and high-mass NS models (see text for details).

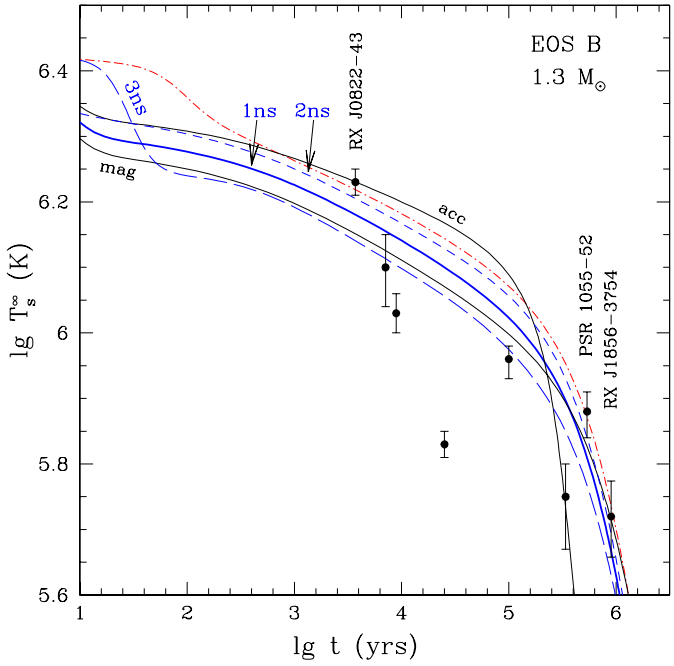

Fig. 10. Cooling curves of $1.3\,M_\odot$ NS model versus observations of RX J0822–43, PSR 1055–52, and RX J1856–3754. Dot-and-dashed curve: proton superfluidity 3p in the NS core. Solid, short-dashed, and long-dashed curves include, in addition, models 1ns, 2ns, and 3ns of crustal neutron superfluidity, respectively. Thick solid line is the same as in Fig. 7. Thin solid curve *acc* is calculated assuming the presence of $2 \times 10^{-11}\,M_\odot$ of hydrogen on the NS surface. Thin solid curve *mag* is obtained assuming the dipole surface magnetic field (10^{12} G at the magnetic pole).

followed by a slow fall at $M \gtrsim M_{\rm D} + 0.003\,M_\odot$. In order to explain these observational limits with the non-superfluid NS models we should make an unlikely assumption that the Vela's mass falls in that narrow mass range. We would face the same difficulty with 1E 1207–52, RX J0002+62, PSR 0656+14, and Geminga. Thus we have five sources which exhibit the intermediate case between the slow and fast cooling. In the absence of superfluidity, this is highly unlikely.

4.2. Proton superfluidity and the three types of cooling neutron stars

Let us explain the observations (Figs. 5–7) by cooling of superfluid NSs. It turns out (Papers I and II) that various superfluids affect NS cooling in different ways. Our main assumptions would be that (i) the *proton superfluidity is rather strong* at $\rho \lesssim \rho_{\rm D}$, while (ii) the $^3{\rm P}_2$ *neutron superfluidity is rather weak* (Sect. 4.4). We will discuss the superfluid effects step by step starting from the effects of proton superfluidity.

The dot-and-dashed cooling curves in Figs. 5–7 are computed assuming the proton superfluidity alone. We adopt the proton pairing 1p in Fig. 5, 2p in Fig. 6, and 3p

in Fig. 7. We use EOS A in the models in Figs. 5 and 6, and EOS B in Fig. 7.

Analyzing Figs. 5–8 we see that, generally, the proton superfluidity leads to the *three* cooling regimes (instead of two): *slow, moderate*, and *fast*. Accordingly, we predict *three types* of cooling NSs with distinctly different properties.

(I) *Low-mass, slowly cooling* NSs. The central densities ρ_c and masses $M = M(\rho_c)$ of these NSs obey the inequalities

$$\rho_c \lesssim \rho_I, \quad M \lesssim M_I = M(\rho_I); \tag{2}$$

the threshold values ρ_I and M_I are specified below.

(II) *Medium-mass, moderately cooling* NSs, with

$$\rho_I \lesssim \rho_c \lesssim \rho_{II}, \qquad M_I \lesssim M \lesssim M_{II} = M(\rho_{II}), \tag{3}$$

ρ_{II} and M_{II} are also specified below.

(III) *Massive, rapidly cooling* NSs,

$$\rho_{II} \lesssim \rho_c \leq \rho_{cmax}, \quad M_{II} \lesssim M \leq M_{max}, \tag{4}$$

where ρ_{cmax} and M_{max} refer to the maximum-mass configuration (Table 1).

We will show that the threshold values of $\rho_{I,II}$ and $M_{I,II}$ depend on a proton superfluidity model, EOS in the NS core, and on a NS age. Let us describe these three cooling regimes in more detail.

(I) We *define the slowly cooling NSs* as those where the direct Urca process is either forbidden by momentum conservation ($\rho_c \leq \rho_D$, Lattimer et al. 1991) or greatly suppressed by the strong proton superfluidity.

In particular, we have the slow cooling for $\rho_c < \rho_D$ and $M < M_D$ in the absence of proton superfluidity. This is the *ordinary* slow cooling discussed widely in the literature. It is mainly regulated by the neutrino energy losses produced by the modified Urca process.

However, for the conditions displayed in Figs. 5–7, the proton superfluidity is so strong that it almost switches off both, the modified Urca process everywhere in the NS core and the direct Urca process at $\rho > \rho_D$. Then the main neutrino emission is produced by *neutrino bremsstrahlung in neutron-neutron collisions* (unaffected by the neutron superfluidity in the NS core that is assumed to be weak). The bremsstrahlung is less efficient than the modified Urca process and leads to an even slower cooling than in a non-superfluid NS. We will refer to it as the *very slow* cooling.

The analysis shows that, for our proton superfluid models, the regime of very slow cooling holds as long as the proton critical temperature in the NS center is higher than a threshold value:

$$T_{cp}(\rho_c) \gtrsim T_{cp}^{(I)}(\rho_c). \tag{5}$$

Comparing the neutrino emissivities of the indicated reactions (e.g., Yakovlev et al. 1999), we can obtain the simple estimates: $T_{cp}^{(I)}(\rho) \sim 5.5\,T$ for $\rho \leq \rho_D$, and $T_{cp}^{(I)}(\rho) \sim 17\,T$ for ρ several per cent higher than ρ_D, where T is the internal NS temperature. There is a continuous transition between the presented values of $T_{cp}^{(I)}(\rho)$ in the narrow density range near ρ_D.

Table 4. Masses $M_{I,II}$ which separate slow, moderate, and rapid cooling models for $t_1 = 4 \times 10^3$ and $t_2 = 4 \times 10^5$ yr.

EOS	Proton pairing	$M_I/M_\odot$		$M_{II}/M_\odot$	
		t_1	t_2	t_1	t_2
A	1p	M_D	1.4	1.52	1.53
A	2p	M_D	1.55	1.64	1.64
A	3p	M_D	1.77	1.83	1.84
B	1p	M_D	M_D	M_D	M_D
B	2p	M_D	M_D	M_D	M_D
B	3p	M_D	1.55	1.62	1.62

To make our analysis less abstract we notice that $T \sim 5.5 \times 10^8$ K in a very slowly cooling NS at $t \sim 4 \times 10^3$ yr, $T \sim 4 \times 10^8$ K at $t \sim 2.5 \times 10^4$ yr, and $T \sim 1.5 \times 10^8$ K at $t \sim 4 \times 10^5$ yr. The dependence of $T_{cp}^{(I)}$ on ρ_c and on the NS age is shown in Fig. 9.

Now we are ready to specify the maximum central densities ρ_I and masses M_I of slowly cooling NSs in Eq. (2). For the cases of study, we have $\rho_I \geq \rho_D$ and $M_I \geq M_D$ because the NSs with $\rho_c < \rho_D$ show slow cooling. If $\rho_c > \rho_D$, then we may find the density ρ_I on the decreasing, high-density slope of $T_{cp}(\rho)$ (Fig. 1) which corresponds to $T_{cp}(\rho_I) = T_{cp}^{(I)}(\rho_I)$ (Fig. 9). It gives the central density of the star and $M_I = M(\rho_I)$. If ρ_I is formally lower than ρ_D, we set $M_I = M_D$.

Table 4 shows the values of M_I for EOSs A and B and proton superfluids 1p, 2p, and 3p at two NS ages, $t_1 = 4 \times 10^3$ yr and $t_2 = 4 \times 10^5$ yr.

According to Fig. 8, a sufficiently strong proton superfluidity smears out a sharp transition from the slow to fast cooling as the mass grows. This effect is illustrated for all three proton superfluid models and EOS A at $t = 2.5 \times 10^4$ yr. In models 2p and 3p the proton superfluidity at the direct Urca threshold is very strong. It drastically suppresses the direct Urca process and makes it unimportant. In these cases, the direct Urca threshold *does not manifest a transition to faster cooling*. Thus, at $t = 2.5 \times 10^4$ yr we have $\rho_I \sim \rho_D$ and $M_I \sim M_D$ for proton superfluid 1p, and we have $\rho_I > \rho_D$, $M_I > M_D$ for superfluids 2p and 3p (Fig. 9).

For the conditions displayed in Figs. 5–7, the cooling curves (dot-and-dashed lines) of all low-mass NSs are very similar. For instance, the $1.35\,M_\odot$ curve in Fig. 5 is plotted just as an example; all the curves are almost identical in the mass range $1.1\,M_\odot \lesssim M < M_I$. Moreover, the curves are not too sensitive to EOS and are *insensitive to the exact values of the proton critical temperature* T_{cp}, as long as the inequality (5) holds. They are noticeably higher than the analogous cooling curves of the ordinary slow cooling in the absence of superfluidity (e.g., Fig. 5).

For the conditions in Figs. 5–7 (as in Papers I and II) we may explain the three relatively hot sources,

RX J0822–43, PSR 1055–52, and RX J1856–3754, by these very-slow-cooling models with a strong proton superfluidity. Thus, we assume that the indicated sources are low-mass NSs. We discuss this explanation further in Sect. 4.3.

(II) We *define the moderately cooling stars* as the NSs which possess central kernels where the direct Urca process is allowed but moderately suppressed by proton superfluidity. The existence of a representative class of these NSs is solely due to proton superfluidity.

Our analysis shows that, for our cooling models, the proton critical temperature in the center of a medium-mass NS should roughly satisfy the inequality

$$T_{\rm cp}^{\rm (II)}(\rho_{\rm c}) \lesssim T_{\rm cp}(\rho_{\rm c}) \lesssim T_{\rm cp}^{\rm (I)}(\rho_{\rm c}), \quad (6)$$

with $T_{\rm cp}^{\rm (II)} \sim 3\,T$. Thus, we may introduce $\rho_{\rm II}$ which corresponds to $T_{\rm cp}(\rho_{\rm II}) = T_{\rm cp}^{\rm (II)}(\rho_{\rm II})$ and determines $M_{\rm II}$, the maximum mass of moderately cooling NSs in Eq. (3). The values of $T_{\rm cp}^{\rm (II)}$ depend mainly on a given EOS and on a NS age (Fig. 9). The ranges of mass and density in Eq. (3) depend also on a model of $T_{\rm cp}(\rho)$.

The values of $M_{\rm II}$ are also given in Table 4, along with $M_{\rm I}$. For EOS B, the critical temperature $T_{\rm cp}(\rho)$ of 1p and 2p proton superfluids vanishes at $\rho \lesssim \rho_{\rm D}$. Then we have a sharp transition from the slow to fast cooling in a narrow mass range just as in the absence of the superfluidity (Sect. 4.1; $M_{\rm I} \approx M_{\rm II} \approx M_{\rm D}$), and the regime of moderate cooling is almost absent.

The surface temperatures of the medium-mass (moderately cooling) NSs are governed by proton superfluidity in the NS central kernels, $\rho \gtrsim \rho_{\rm I}$. One can observe (Figs. 5–8) a steady decrease of surface temperatures with increasing M. If we fix the proton superfluidity and EOS (provided they allow for the moderate cooling) we can determine (Papers I and II) the mass of any moderately cooling NS, which means "weighing" NSs. In this fashion we can weigh five isolated NSs (1E 1207–52, RX J0002+62, Vela, PSR 0656+14, and Geminga) using either EOS A and the proton superfluids 1p, 2p, and 3p, or EOS B and the superfluid 3p. Thus, we assume that the indicated sources are moderately cooling NSs. For instance, adopting EOS A and proton superfluid 1p (Fig. 5) we obtain the masses in the range from $\approx 1.36\,M_\odot$ (for 1E 1207–52) to $\approx 1.465\,M_\odot$ (for Vela and Geminga). For EOS A and proton superfluid 2p (Fig. 6) we naturally obtain higher masses of the same sources. Obviously, the properties of moderately cooling NSs are *extremely sensitive* to the decreasing slope of $T_{\rm cp}(\rho)$ in the temperature range from $T_{\rm cp}^{\rm (II)}$ to $T_{\rm cp}^{\rm (I)}$ (Fig. 9), or in the density range from $\rho_{\rm I}$ to $\rho_{\rm II}$ (and insensitive to the details of $T_{\rm cp}(\rho)$ outside this range).

(III) *Massive* NSs show *fast* cooling similar to the fast cooling of non-superfluid NSs. These stars have central kernels where the direct Urca process is either unaffected or weakly suppressed by the proton superfluidity. In such kernels, $T_{\rm cp}(\rho) \lesssim T_{\rm cp}^{\rm (II)}$. The central densities and masses of rapidly cooling NSs lie in the range given by Eq. (4). The thermal evolution of rapidly cooling NSs is not very sensitive to the model of $T_{\rm cp}(\rho)$ and to EOS in the stellar core. Note that if $\rho_{\rm cmax} < \rho_{\rm II}$, the rapidly cooling NSs do not exist. In the frame of our interpretation, no NS observed so far can be assigned to this class.

4.3. Crustal superfluidity and slow cooling

As the next step, we retain proton superfluidity and add $^1S_0$ neutron superfluidity 1ns in the NS crust and outermost core. In this case we obtain the solid curves in Figs. 5–7. For the moderately or rapidly cooling middle-aged NSs ($M > M_{\rm I}$) they are fairly close to the dot-and-dashed curves. This is quite expected (e.g., Gnedin et al. 2001): the $^1S_0$ neutron superfluidity is mainly located in the NS crust which is much less massive than the NS core. Thus, the crustal superfluidity does not affect noticeably our interpretation of 1E 1207–43, RX J0002+62, Vela, PSR 0656+14, and Geminga in terms of moderately cooling NSs.

However, as pointed out in Paper II, this crustal superfluidity strongly affects the slow cooling of low-mass NSs ($M < M_{\rm I}$). Its effects are twofold. First, at $t \lesssim 3 \times 10^5$ yr the neutrino luminosity due to $^1S_0$ pairing of neutrons may dominate the sufficiently low neutrino luminosity of the stellar core (see Fig. 4 and Paper II, for details). Second, at $t \gtrsim 10^5$ yr the $^1S_0$ neutron superfluidity reduces the heat capacity of the crust. Both effects accelerate NS cooling and decrease $T_{\rm s}^\infty$ (Figs. 5–7) violating our interpretation of the three sufficiently hot sources, RX J0822–43, PSR 1055–52, and RX J1856–3754. The interpretation of RX J1856–3754 is affected to a lesser extent, as a consequence of the rather large errorbar of $T_{\rm s}^\infty$ for this source (Sect. 3).

Let us demonstrate that our interpretation can be rescued by the appropriate choice of $T_{\rm cns}(\rho)$. For this purpose we focus on the interpretation of RX J0822–43, PSR 1055–52, and RX J1856–3754, as the very slowly cooling NSs ($M \leq M_{\rm I}$).

For certainty, let us take EOS B, $M = 1.3\,M_\odot$, and proton superfluid 3p. The results are presented in Fig. 10 (cf. with Fig. 3 of Paper II). The dot-and-dashed line is the same as in Fig. 7 and neglects the crustal neutron superfluidity. Thick solid line is also the same as in Fig. 7. It includes an additional effect of crustal superfluid 1ns and lies below the observational limits on $T_{\rm s}^\infty$ for the sources in question (or almost below in case of RX J1856–3754). To keep the proposed interpretation of the three sources we must raise the cooling curves calculated including the crustal superfluidity. To this aim, we must suppress the neutrino emission associated with $^1S_0$ pairing of neutrons (Fig. 4). Recall that in a middle-aged NS this emission is mainly generated (Fig. 4) in two relatively narrow layers, near the neutron drip point and near the crust-boundary interface, where the local NS temperature T is just below $T_{\rm cns}(\rho)$. Since the Cooper-pairing neutrino luminosity is roughly proportional to the widths of these emitting layers, we can achieve our goal by reducing their widths.

This can be done by setting $T_{\rm cns}^{\rm max}$ higher and by making $T_{\rm cns}(\rho)$ decrease sharper in the wings (see Paper II, for details).

For example, taking crustal superfluid 2ns instead of 1ns (Figs. 1 and 2) we obtain the dashed cooling curve in Fig. 10 which comes much closer to the dot-and-dashed curve than the thick solid curve (model 1ns). (Another example: shifting $T_{\rm cns}(\rho)$ for model 2ns into the crust would additionally raise the curve towards the dot-and-dashed one.) Note that the cooling curves are insensitive to the details of $T_{\rm cns}(\rho)$ profile near the maximum, as long as $T_{\rm cns}^{\rm max} \gtrsim 5\times10^9$ K, but they are extremely sensitive to the decreasing slopes of $T_{\rm cns}(\rho)$. On the other hand, by taking the smoother and lower $T_{\rm cns}(\rho)$, model 3ns, we obtain a colder NS than needed for the interpretation of observations (long-dash line in Fig. 10). Therefore, ^{1}S$_0$ neutron superfluidity with maximum $T_{\rm cns}^{\rm max} < 5\times10^9$ K and/or with smoothly decreasing slopes of the $T_{\rm cns}(\rho)$ profile near the crust-core interface and neutron drip point *violates* the proposed interpretation of the observational data.

Let us stress that the observations of RX J0822–43, PSR 1055–52, and RX J1856–3754 can be fitted even with our initial model 1ns of the crustal neutron superfluidity. The high surface temperature of RX J0822–43 can be explained assuming additionally the presence of a low-mass ($2\times10^{-11}\,M_\odot$) heat-blanketing surface envelope of hydrogen or helium. This effect is modeled using the results of Potekhin et al. (1997). Light elements increase the electron thermal conductivity of NS surface layers and raise $T_{\rm s}^{\infty}$ at the neutrino cooling stage (curve *acc* in Fig. 10). In order to explain the observations of PSR 1055–52 and RX J1856–3754, we can assume again model 1ns of crustal superfluidity, iron surface and the dipole surface magnetic field ($\sim10^{12}$ G at the magnetic pole; line *mag* in Fig. 10). Such a field makes the NS surface layers overall less heat-transparent (Potekhin & Yakovlev 2001), rising $T_{\rm s}^{\infty}$ at $t \gtrsim 3\times10^5$ yr. Note that the dipole field $\gtrsim10^{13}$ G has the opposite effect, resembling the effect of the surface envelope of light elements. Therefore, we can additionally vary cooling curves by assuming the presence of light elements and/or the magnetic field on the NS surface. However, these variations are less pronounced than those due to nucleon superfluidity. For instance, we cannot reconcile the cooling curves with the observations of PSR 1055–52 assuming model 3ns of the crustal superfluidity with any surface magnetic field.

4.4. $^3P_2$ pairing of neutrons in the NS core

Now we focus on the effects of ^{3}P$_2$ neutron pairing, which were neglected so far. They are illustrated in Fig. 5, as an example. They would be qualitatively similar for the other cooling models in Figs. 6 and 7. In Fig. 5 we take the cooling models obtained including proton superfluidity 1p and crustal superfluidity 1ns and add the ^{3}P$_2$ neutron superfluidity (model 1nt, Table 2) in the core. We have the same (solid) cooling curves for the young NSs which have the internal temperatures T above the maximum value of $T_{\rm cnt}^{\rm max} \approx 3\times10^8$ K. However, when T falls below $T_{\rm cnt}^{\rm max}$, we obtain (dots) a strong acceleration of the cooling associated with the powerful neutrino emission due to ^{3}P$_2$ neutron pairing (Fig. 4). This emission complicates our interpretation of older sources, PSR 0656+14, Geminga, PSR 1055–52, and RX J1856–3754. It may induce *really fast cooling* of such sources even if their mass is *low*, $M < M_{\rm D}$ (Sect. 4.2). To avoid this difficulty we assume (Paper I) *weak* ^{3}P$_2$ *pairing*, $T_{\rm cnt}(\rho)$, with maximum $T_{\rm cnt}^{\rm max} < 10^8$ K. Then, it does not affect the proposed interpretation.

5. Summary

Let us summarize the effects of the three types of superfluids on NS cooling:

(a) Strong proton superfluidity in the NS cores, combined with the direct Urca process at $\rho > \rho_{\rm D}$, separates the cooling models into three types: (I) slowly cooling, low-mass NSs ($M \lesssim M_{\rm I}$); (II) moderately cooling, medium-mass NSs ($M_{\rm I} \lesssim M \lesssim M_{\rm II}$); (III) rapidly cooling, massive NSs ($M \gtrsim M_{\rm II}$). These models have distinctly different properties (Sect. 4.2). The regime of moderate cooling cannot be realized without the proton superfluidity.

(b) Strong proton superfluidity in the NS core is required to interpret the observational data on the three sources, RX J0822–43, PSR 1055–52, and RX J1856–3754, hot for their ages, as the very slowly cooling NSs (Sects. 4.2 and 4.3). Within this interpretation, all three sources may have masses from about $1.1\,M_\odot$ to $M_{\rm I}$; it would be difficult to determine their masses exactly or distinguish EOS in the NS core from the cooling models.

(c) Strong proton superfluidity is needed to interpret observations of the other sources, 1E 1207–52, RX J0002+62, Vela, PSR 0656+14, and Geminga, as the medium-mass NSs. This allows one to "weigh" these NSs, i.e., determine their masses, for a given model of $T_{\rm cp}(\rho)$. The weighing is very sensitive to the decreasing slope of $T_{\rm cp}(\rho)$ in the density range $\rho_{\rm I} \lesssim \rho \lesssim \rho_{\rm II}$, and it depends also on the EOS in the NS core (Sect. 4.2).

(d) Strong or moderate ^{3}P$_2$ neutron superfluidity in the NS core initiates rapid cooling due to the neutrino emission resulted from neutron pairing. This invalidates the proposed interpretation of the old sources like PSR 0656+14, Geminga, PSR 1055–52, and RX J1856–3754. To save the interpretation, we assume a weak ^{3}P$_2$ neutron superfluidity, $T_{\rm cnt}^{\rm max} < 10^8$ K (Sect. 4.4).

(e) ^{1}S$_0$ neutron superfluidity in the crust may initiate a strong Cooper-pairing neutrino emission, decrease substantially $T_{\rm s}^{\infty}$ of the slowly cooling NSs, and weaken our interpretation of RX J0822–43, PSR 1055–52, and RX J1856–3754 (although it does not affect significantly the moderate or fast cooling). We can save the interpretation by assuming that the maximum of the critical temperature profile $T_{\rm cns}(\rho)$ is not too small ($T_{\rm cns}^{\rm max} \gtrsim 5\times10^9$ K) and the profile decreases sharply in the wings (Sect. 4.3).

(f) The interpretation of the slowly cooling sources is sensitive to the presence of the surface magnetic fields and/or heat-blanketing surface layer composed of light elements (Sect. 4.3).

(g) No isolated middle-aged NSs observed so far can be identified as a rapidly cooling NS. In the frame of our models, these NSs do not exist for those EOSs and superfluid $T_{\rm cp}(\rho)$ for which $M_{\max} < M_{\rm II}$.

If our interpretation is correct, we can make the following conclusions on the properties of dense matter in NS interiors.

(i) Strong proton superfluidity we need is in favor of a not too large symmetry energy at supranuclear densities (Paper I). A very large symmetry energy would mean a high proton fraction which would suppress proton pairing. On the other hand, the symmetry energy should not be too small to open the direct Urca process at $\rho > \rho_{\rm D}$.

(ii) Weak $^3{\rm P}_2$ neutron pairing is in favor of a not too soft EOS in the NS core (Paper I). The softness would mean a strong attractive nn interaction and, therefore, strong neutron pairing.

(iii) Specific features of the crustal neutron superfluidity we adopt are in favor of those microscopic theories which predict $T_{\rm cns}(\rho)$ profiles with $T_{\rm cns}^{\max} \gtrsim 5 \times 10^9$ K (or $\Delta_{\rm cn}(k)$ profiles with $\Delta_{\rm cn}^{\max} \gtrsim 1$ MeV, see Fig. 2). This is in line with many microscopic calculations of the superfluid gaps which include the medium polarization effects in nn interaction (e.g., Lombardo & Schulze 2001). However, the reduction of the gap by the medium polarization should not be too strong, and the decreasing slope of $\Delta(k)$ should be rather sharp. These requirements constrain the microscopic theories.

The proposed interpretation of the observations relates the inferred NS masses to the superfluid properties of NS interiors. By varying EOS and the proton critical temperature, we can attribute different masses to the same sources. If, on the other hand, we knew the range of masses of the cooling middle-aged NSs we would be able to draw definite conclusions on the superfluid state of their interiors, first of all, on the proton critical temperature, $T_{\rm cp}(\rho)$.

Our analysis may seem too simplified because we neglect a possible presence of other particles in the NS cores (muons, hyperons, quarks). We expect that the inclusion of other particles and the effects of superfluidity of hyperons or quarks will complicate theoretical analysis but will not change our basic conclusion on the existence of the slowly, moderately, and rapidly cooling NSs.

Our calculations show that the cooling of middle-aged NSs with $M < M_{\rm I}$ is sensitive to the density profile of free neutrons near the crust bottom and neutron drip point. We have used only one model of the free-neutron distribution in the crust, assuming the atomic nuclei to be spherical at the crust bottom. It would be interesting to consider the models of crust matter with non-spherical nuclei (e.g., Pethick & Ravenhall 1995) and the effects of superfluidity of nucleons confined in the atomic nuclei in the NS crust.

Let us stress that determination of $T_{\rm s}^{\infty}$ from observational data is a very complicated problem (as described in part by Yakovlev et al. 1999). It requires very high-quality data and theoretical models of NS atmospheres. Thus, the current values of $T_{\rm s}^{\infty}$ may change substantially after the forthcoming observations and new theoretical modeling. These changes may affect our interpretation of the observational data, first of all, of RX J0822–43, PSR 1055–52, and RX J1856–3754. For instance, RX J1856–3754 may have a colder surface ($T_{\rm s}^{\infty} \sim 0.25$ MK), than assumed in the above analysis, with a hot spot (e.g., Pons et al. 2001; Burwitz et al. 2001; Gänsicke et al. 2001). If confirmed, the lower $T_{\rm s}^{\infty}$ might be explained by the effect of $^3{\rm P}_2$ neutron pairing (Fig. 5). We expect that future observations of the thermal emission from these sources will be crucial for understanding the superfluid properties of NS matter.

Acknowledgements. We are grateful to G. G. Pavlov for encouragement, to M. E. Gusakov, K. P. Levenfish, and A. Y. Potekhin for critical remarks, and to P. Haensel, our coauthor of Paper I, for useful comments. One of the authors (DGY) is grateful to the Institute for Nuclear Theory at the University of Washington for its hospitality and to the Department of Energy for partial support during the completion of this work. The work was partially supported by RFBR (grant No. 99-02-18099).

References

Burwitz, V., Zavlin, V. E., Neuhäuser, R., et al. 2001, A&A, 327, L35
Craig, W. W., Hailey, Ch. J., & Pisarski, R. L. 1997, ApJ, 488, 307
Gänsicke, B. T., Braje, T. M., & Romani, R. W. 2001, A&A, submitted [astro-ph/0110130]
Gnedin, O. Y., Yakovlev, D. G., & Potekhin, A. Y. 2001, MNRAS, 324, 725
Flowers, E. G., Ruderman, M., & Sutherland, P. G. 1976, ApJ, 205, 541
Halpern, J. P., & Wang, F. Y.-H. 1997, ApJ, 477, 905
Kaminker, A. D., Haensel, P., & Yakovlev, D. G. 2001, A&A, 373, L17, Paper I
Kaplan, D. L., van Kerkwijk, M. H., & Anderson, J. 2001, ApJ, submitted [astro-ph/0111174]
Lattimer, J. M., Pethick, C. J., Prakash, M., & Haensel, P. 1991, Phys. Rev. Lett., 66, 2701
Lattimer, J. M., Van Riper, K. A., Prakash, M., & Prakash, M. 1994, ApJ, 425, 802
Lattimer, J. M., & Prakash, M. 2001, ApJ, 550, 426
Lyne, A. G., Pritchard, R. S., Graham-Smith, F., & Camilo, F. 1996, Nature, 381, 497
Lombardo, U., & Schulze, H.-J. 2001, in Physics of Neutron Star Interiors, ed. D. Blaschke, N. Glendenning, & A. Sedrakian (Springer, Berlin), 31
Negele, J. W., & Vautherin, D. 1973, Nucl. Phys. A, 207, 298
Ögelman, H. 1995, in Lives of Neutron Stars, ed. M. A. Alpar, Ü. Kiziloğlu, & J. van Paradjis, NATO ASI Ser. (Kluwer, Dordrecht), 101
Page, D., & Applegate, J. H. 1992, ApJ, 394, L17

Pavlov, G. G., Zavlin, V. E., Sanwal, D., Burwitz, V., & Garmire, G. P. 2001, ApJ, 552, L129
Pethick, C. J., & Ravenhall, D. G. 1995, Ann. Rev. Nucl. Particle Sci., 45, 429
Pons, J., Walter, F., Lattimer, J., et al. 2001, ApJ, 564, 981
Possenti, A., Mereghetti, S., & Colpi, M. 1996, A&A, 313, 565
Potekhin, A. Y., Chabrier, G., & Yakovlev, D. G. 1997, A&A, 323, 415
Potekhin, A. Y., & Yakovlev, G. G. 2001, A&A, 374, 213
Prakash, M., Ainsworth, T. L., & Lattimer, J. M. 1988, Phys. Rev. Lett., 61, 2518
Schulze, H.-J., Cugnon, J., Lejeune, A., Baldo, M., & Lombardo, U. 1996, Phys. Lett. B, 375, 1
Walter, F. M. 2001, ApJ, 549, 433
Wambach, J., Ainsworth, T. L., & Pines, D. 1993, Nucl. Phys. A, 555, 128
Yakovlev, D. G., Levenfish, K. P., & Shibanov, Yu. A. 1999, Physics–Uspekhi 42, 737 [astro-ph/9906456]
Yakovlev, D. G., Kaminker, A. D., Gnedin, O. Y., & Haensel, P. 2001, Phys. Rep., 354, 1
Yakovlev, D. G., Kaminker, A. D., & Gnedin, O. Y. 2001, A&A, 379, L5, Paper II
Zavlin, V. E., Pavlov, G. G., & Trümper, J. 1998, A&A, 331, 821
Zavlin, V. E., & Pavlov, G. G. 1999, private communication
Zavlin, V. E., Trümper, J., & Pavlov, G. G. 1999, ApJ, 525, 959